CrossMark

Modeling mono- and multi-component adsorption of cobalt(II), copper(II), and nickel(II) metal ions from aqueous solution onto a new carboxylated sugarcane bagasse. Part I: Batch adsorption study

Stela Nhandeyara do Carmo Ramos [a], Amália Luísa Pedrosa Xavier [a],
Filipe Simões Teodoro [a], Megg Madonyk Cota Elias [a], Fernanda Jorge Gonçalves [a],
Laurent Frédéric Gil [a], Rossimiriam Pereira de Freitas [b], Leandro Vinícius Alves Gurgel [a,*]

[a] Group of Physical Organic Chemistry (GPOC), Department of Chemistry, Institute of Biological and Exact Sciences (ICEB), Federal University of Ouro Preto, Campus Morro do Cruzeiro, Bauxita, 35400-000 Ouro Preto, Minas Gerais, Brazil
[b] Department of Chemistry, Institute of Exact Sciences (ICEx), Federal University of Minas Gerais, Avenida Antônio Carlos, 6627, 31270-901 Belo Horizonte, Minas Gerais, Brazil

ABSTRACT

A new carboxylated-functionalized sugarcane bagasse (STA) was prepared through the esterification of sugarcane bagasse with trimellitic anhydride. The optimized synthesis conditions yield STA with a percent weight gain of 73.9% and the number of carboxylic acid groups accounted for 3.78 mmol/g. STA was characterized by FTIR, elemental analysis, TGA, PZC, and SEM. Adsorption kinetics followed a pseudo-second-order model. The adsorption rate constant showed the following order: $k_{2,\text{Ni}^{2+}} > k_{2,\text{Cu}^{2+}} > k_{2,\text{Co}^{2+}}$. Four mono- and multi-component isotherm models were used to model the adsorption systems. Mono-component experimental data were fitted to Langmuir and Sips models; whereas, multicomponent data were fitted to modified extended Langmuir and *P*-factor models. The maximum adsorption capacities ($Q_{\text{max,mono}}$) obtained from the Langmuir model were 1.140, 1.197, and 1.563 mmol/g for Co^{2+}, Cu^{2+}, and Ni^{2+}, respectively. The competitive studies demonstrated that the multicomponent adsorption capacity ($Q_{\text{max,multi}}$) was smaller than $Q_{\text{max,mono}}$, as a result of the interaction between the metal ions. Desorption studies showed that all metal ions could be fully desorbed from STA.

© 2015 Elsevier B.V. All rights reserved.

1. Introduction

The Agency for Toxic Substances and Disease Registry (ATSDR, 2014) have classified some metals as toxic, persistent, and bioaccumulative elements. Among the most hazardous substances that impose risks to human health are various toxic metals (Ahmad and Prasad, 2011). Interestingly, arsenic (As), lead (Pb), and mercury (Hg) are the top three most harmful metals, followed by cobalt (Co), nickel (Ni), and copper (Cu) at positions 51, 57, and 118, respectively (Ahmad and Prasad, 2011; ATSDR, 2014). Such toxic metals are present in the ionic form in waste streams from mining operations, tanneries, batteries, electronics, electroplating, and petrochemicals as well as in textile and pesticide mills (Amin et al., 2013; Fu and Wang, 2011; Kazemipour et al., 2008). Toxic metals are some of the major pollutants in marine, soil, solid industrial wastes, and

untreated industrial wastewaters. Both solid and liquid industrial wastes can be considered as major sources of innumerous types of metals found in soil, groundwater, and water bodies (Amin et al., 2013; Kazemipour et al., 2008). The discharge of industrial effluents containing large amounts of toxic metals into the environment without suitable treatment has resulted in serious environmental problems (Amin et al., 2013; Barakat, 2011; Soetan et al., 2010).

Co, Cu, and Ni are all micronutrients for plants, animals, and humans (Ahmad and Prasad, 2011; Soetan et al., 2010). They participate in prosthetic groups and as co-factors of many enzymes and are, therefore, essential; however, at high concentrations, they can cause several serious health problems in humans (Ahmad and Prasad, 2011). The toxic effects of Co, Cu, and Ni are well documented (Klaassen, 2008).

Various physicochemical methods have been suggested for the removal of metal ions from industrial wastewaters such as electrochemical and chemical precipitation, ultrafiltration and nanofiltration, ion exchange, and reverse osmosis (Fu and Wang, 2011; Kazemipour et al., 2008). Such methods can be adopted

---

alone or in combination, such as chemical precipitation followed by nanofiltration (Fu and Wang, 2011). Such processes have significant drawbacks, such as incomplete removal, high-energy requirements, and production of toxic sludge that needs to be treated and disposed (Barakat, 2011).

Recently, various studies have reported the development of cheaper and more effective technologies, aiming to decrease the amount of wastewater produced and enhance the standard quality of the treated effluent (Barakat, 2011; Fu and Wang, 2011). Adsorption has become one of the cheaper alternative treatments, as the search for low-cost adsorbents (modified or not) with a metal ion-binding capacity has been intensified (Bhatnagar and Sillanpää, 2010; Miretzky and Cirelli, 2010; Sun, 2010; Wan Ngah and Hanafiah, 2008). Agricultural by-products are promising candidates as effective adsorbents, owing to their low cost and availability throughout the world (Kumar, 2006). Among the most important low-cost agricultural by-products is sugarcane bagasse (SB). It is largely available in countries such as Brazil, China, and India, where it is a by-product from the sugar and bioethanol mills. Among these countries, Brazil is the world's largest producer of sugarcane (Ferreira et al., 2015). SB is mainly composed of cellulose ($42.19 \pm 1.93\%$), hemicelluloses ($27.60 \pm 0.88\%$), lignin ($21.56 \pm 1.67\%$), ash ($5.63 \pm 2.31\%$), and extractives ($2.84 \pm 1.22\%$) (Rocha et al., 2015). The three major components of SB are rich in primary and secondary hydroxyl groups that can be used to graft functional groups with a metal ion-binding capacity (Wan Ngah and Hanafiah, 2008).

This study aimed to prepare a new adsorbent with an improved metal ion-binding capacity from chemical modification of SB with trimellitic anhydride (TA). TA is a commercial and stable reagent. After esterification with SB, it releases two carboxylic acid groups that can form complexes with different metal ions. The chemical modification of SB was intensively studied and optimized. The new adsorbent material was used to study the removal of Co^{2+}, Cu^{2+}, and Ni^{2+} from spiked monocomponent and multicomponent aqueous solutions. The influence of time, pH, and metal ion concentration on adsorption was studied in detail. Desorption and reuse of the spent adsorbent was also evaluated.

2. Experimental

2.1. Materials

$CoCl_2 \cdot 6H_2O$, $CuSO_4 \cdot 5H_2O$, $CH_3COONa \cdot 3H_2O$, monochloroacetic acid (99%), and isopropanol were purchased from Synth (Brazil). 1,2,4-Benzenetricarboxylic anhydride (trimellitic anhydride, TA) (97%) (cat no. 552-30-7) and 3 Å molecular sieve (cat no. 208582) were purchased from Sigma–Aldrich (Brazil). $NiCl_2 \cdot 6H_2O$, glacial acetic acid (99.5%), NaOH, HCl (37% w/w), acetone, N,N'-dimetylacetamide (DMA), and pyridine (Py) were purchased from Vetec (Brazil). Quantitative filter papers (blue ribbon, JP 41, cat no. 3509-1, 12.5 cm diameter, ash content of 0.00009 g, and grammage of 80 g/cm^2) were purchased from JProlab (Brazil). Before use, DMA was stored with molecular sieves (3 Å) that had been previously activated in an oven at 150 °C. Py was refluxed in a round-bottomed flask with NaOH pellets for 12 h and distilled before use.

2.2. Sugarcane bagasse preparation

SB stalks were provided by a local sugar and alcohol company, Ouro Preto, Minas Gerais, Brazil. The SB was dried under sunlight for 1 week, cut into 100 mm pieces, and milled in a wiley mill (DeLeo Brazil) to pass a 16-mesh screen. The SB was sifted on an electromagnetic stirrer (Bertel, Brazil) using a three-sieve system composed of 16 (1.00 mm), 60 (0.251 mm), and 100 (0.149 mm) mesh for 10 min when set to vibrate with an amplitude of 1. The fraction retained by the 60-mesh screen was collected, transferred to a 5 L beaker, suspended, and stirred using a magnetic stirrer in distilled water at 70 °C for 1 h to remove water-soluble compounds. The SB was then washed with distilled water, and acetone before being dried in an oven at 90 °C. To remove SB extractives, that is, phenolic compounds, it was washed in Soxhlet apparatus with hexane/ethanol (1:1, v/v) for 4 h, dried in an oven at 90 °C to remove the organic solvents, and stored in a desiccator prior to use.

2.3. Preparation of SB modified with trimellitic anhydride (STA)

The chemical modification of SB with TA to obtain STA was optimized by studying the effect of reaction time and TA amount on the percent weight gain (pwg) and number of carboxylic acid groups (n_{COOH}).

2.3.1. Modification of SB as a function of the amount of TA

SB (1.0 g), different amounts of TA (2.0, 4.0, 6.0 and 8.0 g), anhydrous DMA (7.5 mL), and anhydrous Py (7.5 mL) were added to a round-bottomed flask to give a solid-to-liquid ratio of 1:15 (w/v) (SB:DMA/Py). Then, the flask was equipped with a reflux condenser attached to a drying tube packed with anhydrous calcium chloride. The suspensions were heated at 100 °C in an oil bath under constant magnetic stirring (300 rpm) (Corning®, model PC-420D) for 3 h. At the end of each reaction, the suspensions were left to cool (30 min) and were then transferred to 250 mL beakers containing 125 mL of isopropanol. The suspensions were magnetically stirred for 30 min before being transferred to a sintered glass funnel (150 mL, porosity 3). This procedure was performed twice, using a total of 250 mL of isopropanol. Then, STAs were washed in a row with distilled water (100 mL), 0.01 mol/L HCl solution (100 mL), distilled water (100 mL), and isopropanol (50 mL). The yellow solids (STAs) were dried in an oven at 95 °C for 2.5 h, put in a desiccator to cool, and weighed. The pwg and n_{COOH} values were determined.

2.3.2. Modification of SB as a function of reaction time

SB (1.0 g), TA (4.0 g), anhydrous DMA (7.5 mL), and anhydrous Py (7.5 mL) were added to a round-bottomed flask to give a solid-to-liquid ratio of 1:15 (w/v). Then, the flask was equipped with a reflux condenser attached to a drying tube packed with anhydrous calcium chloride. The suspensions were heated at 100 °C in an oil bath under constant magnetic stirring (300 rpm) (Corning®, model PC-420D). Different reaction times were studied 1, 3, 6, 12, 18, 24, and 30 h. The purification and characterization of STAs followed the same procedure described in Section 2.3.1.

2.4. Characterization of STA

2.4.1. Percent weight gain (pwg)

The pwg after chemical modification of SB with TA was calculated using Eq. (1).

$$pwg = \left(\frac{w_{STA} - w_{SB}}{w_{SB}} \right) \times 100 \qquad (1)$$

where pwg (%) is the percent weight gain, and w_{STA} and w_{SB} (g) are the weights of STA and SB after and before chemical modification, respectively.

2.4.2. Number of carboxylic acid groups (n_{COOH})

The n_{COOH} of STA was determined by acid-base back titration. Two 0.1000 g samples of STA were weighed into 250 mL Erlenmeyer flasks and 100.0 mL of standardized NaOH solution (10 mmol/L) was added to each Erlenmeyer flask. The flasks were mechanically stirred at 25 °C for 60 min at 100 rpm. The suspensions were filtered off using a single filtration (JP 41 filter paper). Three 20.0 mL

aliquots from each Erlenmeyer flask were titrated with standardized HCl solution (10 mmol/L) until the phenolphthalein endpoint. The n_{COOH} of STA was calculated using Eq. (2).

$$n_{COOH} = \frac{[C_{NaOH}V_{NaOH} - f(C_{HCl}V_{HCl})]}{w_{STA}} \qquad (2)$$

where n_{COOH} (mmol/g) is the number of carboxylic acid groups on STA, C_{NaOH} and C_{HCl} (mmol/L) are the concentrations of standardized NaOH and HCl solutions, respectively, V_{NaOH} (L) is the volume of standardized NaOH solution, V_{HCl} (L) is the volume of standardized HCl solution expended titrating the excess of unreacted NaOH, w_{STA} (g) is the weight of SB modified with TA, and f is a conversion factor ($f = 5$).

2.4.3. Determination of the point of zero charge (PZC)

To determine the PZC of STA, three different initial pH solutions (3, 6, and 11) were prepared using 0.1 mol/L HNO₃ and 0.1 mol/L NaOH solutions (Noh and Schwarz, 1990). For each initial pH, 20.0 mL of 0.01 mol/L NaNO₃ solution (background electrolyte) and different amounts of STA samples were added to five 125 mL Erlenmeyer flasks to give suspensions of 0.05, 0.1, 0.5, 1, and 2% (w/v). The flasks were mechanically stirred at 25 °C for 24 h at 130 rpm (Nova Ética, model 109/2). The equilibrium pH was measured using a pH meter (Hanna Instruments, model HI 223).

2.4.4. Fourier transform infrared (FTIR) spectroscopy

SB and STA were analyzed by FTIR spectroscopy. Samples were previously dried in an oven at 90 °C for 1 h. Then, 1.0 mg of SB, STA, STA-loaded with Co²⁺, Cu²⁺, and Ni²⁺, and STA after desorption of Co²⁺, Cu²⁺, and Ni²⁺ were mixed with 100.0 mg of spectroscopy grade KBr and pressed in a hydraulic press at 8 tons for 0.5 min to prepare 13 mm KBr pellets (Pike CrushIR, model 181-1110, Pike Technologies, Canada). The FTIR spectra were recorded on an ABB Bomen MB 3000 FTIR spectrometer (Quebec, Canada) equipped with ZnSe optics and a DTGS detector at a resolution of 4 cm⁻¹ from 500 to 4000 cm⁻¹ with 32 scans per sample.

2.4.5. Elemental analysis

The carbon (C), hydrogen (H), and nitrogen (N) contents in SB and STA were determined by elemental analysis. Samples were previously dried in an oven at 90 °C for 1 h. Elemental analysis was performed on a PerkinElmer Series II CHNS/O 2400 analyzer (Shelton, USA).

2.4.6. Thermogravimetric analysis (TGA)

TGA curves were recorded on a Shimadzu DTG-60H simultaneous TG–DTA thermogravimetric analyzer on an alumina pan under a nitrogen atmosphere at a flow rate of 100 mL/min from 35 to 700 °C at a linear heating rate of 10 °C/min. Samples of SB and STA were previously dried in an oven at 90 °C for 1 h.

2.4.7. Scanning electron microscopy (SEM)

Morphologies of SB and STA were examined on a Vega3 SB scanning electron microscope (Tescan/Oxford Instruments) with a filament voltage of 20 keV and secondary electron (SE) detector. Samples of SB and STA were previously dried in an oven at 90 °C for 1 h. Samples of SB and STA were placed on a graphite ribbon that was fixed on aluminum sample holders and sputter-coated with gold in a modular high-vacuum coating Q150R ES (Quorum Technologies).

2.4.8. Energy dispersive X-ray (EDX) spectroscopy

The surface of the STA adsorbent loaded with Co²⁺, Cu²⁺, and Ni²⁺ was mapped on a Vega3 SB SEM–EDX spectrometer (Tescan/Oxford Instruments) with a filament voltage of 20 keV and backscattered electron (BSE) detector. Samples of STA loaded with metal ions were previously dried in an oven at 60 °C for 12 h. Samples of STA–Co²⁺, Cu²⁺, and Ni²⁺ (100 mg) were pressed in a hydraulic press at 8 tons for 1 min to prepare 13 mm pellets. The samples were sputter-coated with carbon in a modular high-vacuum coating Q150R ES (Quorum Technologies).

2.5. Adsorption experiments

STA adsorbent was used for Co²⁺, Cu²⁺, and Ni²⁺ adsorption in aqueous mono- and multi-component solutions in batch mode. Adsorption was studied as a function of time (kinetics), pH, and initial metal ion concentration.

2.5.1. Adsorption of metal ions on STA as a function of contact time (kinetics)

Samples with 100.0 mL of 0.79 mmol/L metal ion solution buffered at pH 5.5 for Cu²⁺ and 5.75 for Co²⁺ and Ni²⁺ using 0.05 mol/L CH₃COOH/CH₃COONa were added to 250 mL Erlenmeyer flasks and pre-thermostated to 25 °C in a shaker incubator for 1 h (Tecnal, model TE-424, Piracicaba, SP, Brazil). Then, 20.0 mg samples of STA were weighed on cylindrical glasses (1.8 mm height and 2.2 mm diameter), added to each Erlenmeyer flask and stirred at 130 rpm for different time intervals. After shaking, the solids were filtered off by a single filtration (JP 41 filter paper) and the metal ion concentration was determined by flame atomic absorption spectrophotometry (FAAS) ($\lambda_{Co} = 240.7$ nm, $\lambda_{Cu} = 324.8$ nm, and $\lambda_{Ni} = 232$ nm). The amount of each metal ion adsorbed on STA in each time was calculated using Eq. (3).

$$q_t = \frac{(C_{i,M^{2+}} - C_{t,M^{2+}})V_{M^{2+}}}{w_{STA}} \qquad (3)$$

where q_t (mmol/g) is the amount of metal ion (M^{2+}) adsorbed per weight of STA at time t, $V_{M^{2+}}$ (L) is the volume of metal ion solution, $C_{i,M^{2+}}$ and $C_{t,M^{2+}}$ (mmol/L) are the concentrations of metal ion solution at 0 and time t, and w_{STA} (g) is the weight of STA adsorbent.

2.5.2. Adsorption of metal ions on STA as a function of pH

STA samples (20.0 mg) were weighed into 250 mL Erlenmeyer flasks and 100.0 mL of 0.79 mmol/L metal ion solution was added. Metal ion solutions were buffered at pH values from 2.0 to 3.5 using 0.05 mol/L ClCH₂COOH/ClCH₂COONa solutions and from 4.0 to 5.75 using 0.05 mol/L CH₃COOH/CH₃COONa solutions. The Erlenmeyer flasks were transferred to a pre-thermostated shaker incubator at 25 °C and mechanically stirred at 130 rpm until equilibrium was reached. After shaking, the solids were filtered off by a single filtration (JP 41 filter paper) and the metal ion concentration was determined by FAAS. The solubility product constant (K_{sp}) for Co(OH)₂ (5.92×10^{-15}), Cu(OH)₂ (1.8×10^{-20}), and Ni(OH)₂ (5.48×10^{-16}) were used to calculate the maximum pH value of the metal ion solutions to avoid the formation of hydrolyzed species and precipitation (Haynes, 2014).

2.5.3. Adsorption isotherms
2.5.3.1. Monocomponent.

STA samples (20.0 mg) were weighed into 250 mL Erlenmeyer flasks and 100.0 mL of each metal ion solution (buffered at pH 5.5 for Cu²⁺ and 5.75 for Co²⁺ and Ni²⁺ with 0.05 mol/L CH₃COOH/CH₃COONa solution), with concentrations ranging from 0.05 to 1.12 mmol/L, were added. Further procedures were the same described in Sections 2.5.1 and 2.5.2.

2.5.3.2. Multicomponent.

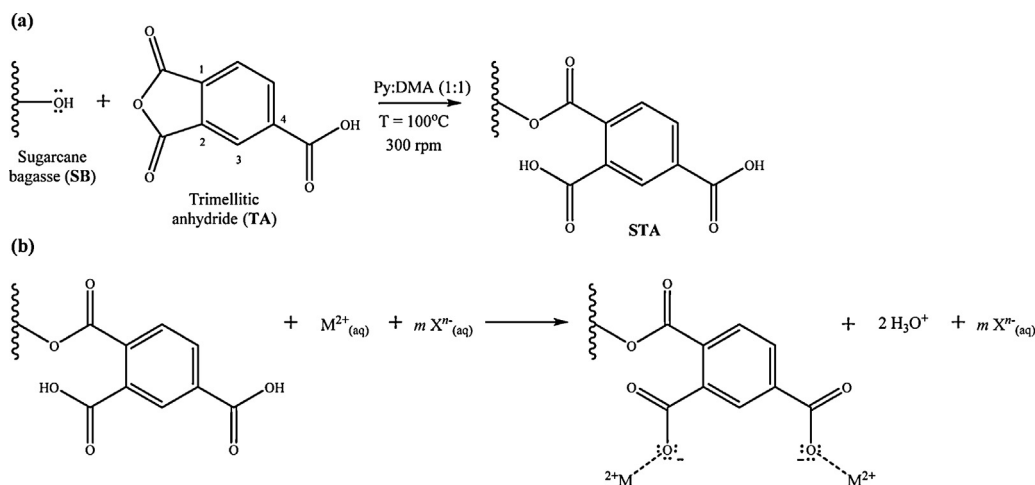STA samples (20.0 mg) were weighed into 250 mL Erlenmeyer flasks and 100.0 mL of binary equimolar metal ion solutions

Fig. 1. (a) Scheme illustrating the synthesis strategy used to prepare STA and (b) suggested mechanism of adsorption of metal ions (M^{2+}) on STA adsorbent (M = Co, Cu, or Ni and mX^{n-} = counter ion (SO_4^{2-} or Cl^-)).

Table 1
The results of optimizing the chemical modification of SB with TA.

Trimellitic anhydride (TA) (g)	Reaction time (h)	STA[a]	
		pwg (%)	n_{COOH} (mmol/g)
1.0	3	16.79 ± 1.42	1.91 ± 0.01
2.0		42.91 ± 2.40	2.97 ± 0.02
4.0		60.72 ± 3.11	3.75 ± 0.01
6.0		64.93 ± 1.26	3.74 ± 0.16
4.0	1	47.61 ± 0.93	3.10 ± 0.08
	3	60.72 ± 3.11	3.75 ± 0.01
	6	63.98 ± 0.60	4.20 ± 0.10
	12	71.00 ± 3.14	4.08 ± 0.01
	18	77.55 ± 3.35	4.78 ± 0.19
	24	88.55 ± 0.89	4.72 ± 0.03
	30	64.69 ± 1.63	4.49 ± 0.13

[a] The weight of SB used in all chemical modifications was 1.0 g. All reactions were performed in duplicate.

(buffered at pH 5.5 with 0.05 mol/L CH_3COOH/CH_3COONa solution), with concentrations ranging from 0.05 to 1.12 mmol/L for Co^{2+}–Ni^{2+}, Cu^{2+}–Ni^{2+}, and Co^{2+}–Cu^{2+}, were added. Further procedures were the same described in Sections 2.5.1 and 2.5.2.

2.6. Desorption experiments

STA samples (100.0 mg) were loaded with 100.0 mL of buffered metal ion solution (3.15 mmol/L for Co^{2+}, Cu^{2+}, and Ni^{2+}) at pH 5.5 (0.05 mol/L CH_3COOH/CH_3COONa solution) for 180, 250, and 75 min, that is, the optimal parameters determined from adsorption studies for Co^{2+}, Cu^{2+}, and Ni^{2+}, respectively. Samples of STA-loaded with each metal ion were recovered by a single filtration, washed with an excess of deionized water (Millipore, model Milli-Q™ Simplicity™) to remove metal ions that were not adsorbed on STA, dried in an oven at 60 °C for 12 h, and weighed. Dried samples of STA (20.0 mg) loaded with each metal ion were weighed into 250 mL Erlenmeyer flasks and 20.0 mL of aqueous desorption solution (1.0 mol/L HNO_3) was added. The Erlenmeyer flasks were transferred to a pre-thermostated shaker incubator at 25 °C and mechanically stirred at 130 rpm for 5 min. Further procedures were the same described in Sections 2.5.1 and 2.5.2. The desorption efficiency (E_{des}) of each STA-metal ion system was calculated using Eq. (4).

$$E_{des} = \left(\frac{C_{e,M^{2+}} V}{Q_{T,max} w_{STA}} \right) \times 100 \qquad (4)$$

where E_{des} (%) is the desorption efficiency, $C_{e,M}^{2+}$ (mmol/L) is the equilibrium concentration of M^{2+} in aqueous desorption solution, V (L) is the volume of desorption solution, $Q_{T,max}$ (mmol/g) is the theoretical maximum adsorption capacity calculated for each metal ion, and w_{STA} (g) is the weight of STA-loaded with each metal ion.

2.6.1. Reuse of the spent adsorbent after desorption

Samples of 20.0 mg of STA (dried in an oven at 80 °C for 1 h) from the desorption study were weighed into 250 mL Erlenmeyer flasks and 100.0 mL of 0.79 mmol/L metal ion solution was added. The optimal parameters determined from adsorption studies were used. Further procedures were the same as those described in Sections 2.5.1 and 2.5.2. The re-adsorption efficiency (E_{re-ads}) of STA for a cycle of adsorption of metal ion after desorption was calculated using Eq. (5).

$$E_{re-ads} = \frac{\left\{ \left[\left(w_{STA,M^{2+}} - w_{STA} \right) Q_{T,max} \right]_{des} + (Q_{max} w_{STA})_{ads} \right\} / w_{STA}}{Q_{T,max}}$$
$$\times 100 \qquad (5)$$

where E_{re-ads} (%) is the re-adsorption efficiency, $w_{STA,M}^{2+}$ (g) is the weight of STA-loaded with metal ions, w_{STA} (g) (inside brackets with subscript des) is the weight of STA after desorption (determined from $w_{STA,M}^{2+}$ and the desorption efficiency, E_{des}), Q_{max} (mmol/g) is the new maximum adsorption capacity obtained from re-adsorption study, and w_{STA} (g) is the weight of STA used in the re-adsorption study. The subscripts des and ads in Eq. (5) are related to the desorption and re-adsorption experiments.

3. Results and discussions

3.1. Synthesis and characterization of STA

3.1.1. Percent weight gain (pwg) and number of carboxylic acid groups (n_{COOH})

Fig. 1 shows the synthetic strategy used to prepare the STA adsorbent and a suggested adsorption mechanism for metal ions (M^{2+}) on STA. The modification of SB with TA using Py as the base/catalyst and DMA as the solvent to obtain STA was optimized by studying the effects of reaction time and TA amount on the pwg and n_{COOH} values. The results of the reaction optimization are shown in Table 1, which shows that, as the amount of TA was increased, pwg and n_{COOH} also increased. The increase in the amount of TA from 4.0 to 6.0 g yielded a small increase in the pwg, but the value of n_{COOH} was almost the same, considering the standard deviation. Thus, 4.0 g of TA was chosen as the best amount to obtain the highest n_{COOH} for the subsequent experiments as a function of reaction time. As the reaction time increased, pwg and n_{COOH} also increased until 24 h. After 24 h, both pwg and n_{COOH} decreased, which is probably because of the chemical degradation of STA caused by the longer heating time. A longer heating time may also allow diesterification reactions, which could diminish the weight gain caused by the release of water molecules. Water molecules can also hydrolyze the ester bonds between hydroxyl groups of SB and the trimellitate moiety, allowing a decreasing in both pwg and n_{COOH}. Furthermore, longer reaction times can substantially increase the preparation cost of STA. Therefore, taking into account the obtained results, a reaction time of 6 h and a TA-to-SB ratio of 4:1 were chosen to prepare a larger amount of STA in order to accomplish the adsorption experiments. When increasing the scale of the reaction to 10.0 g of SB and 40.0 g of TA, pwg and n_{COOH} became 73.9% and 3.78 ± 0.03 mmol/g, respectively. The scale-up of the reaction resulted in a pwg increase of 15.5% and a n_{COOH} decrease of 11.1%. The estimated preparation cost of STA (TA/SB ratio of 4:1 and reaction time of 6 h), considering the international market prices of the chemicals used, SB, and electricity in Brazil, was US\$ 57.43 per kilogram of STA. This preparation cost did not include the elaboration steps described in Section 2.3.1.

3.1.2. Elemental analysis and FTIR spectroscopy

Elemental and FTIR spectroscopy analyses were performed for unmodified SB and TA-modified SB. The carbon, hydrogen, nitrogen, and oxygen contents for SB and STA were 46.56 and 52.45%, 5.09 and 4.10%, 0.30 and 0.97%, and 48.06 and 42.49%, respectively. The oxygen content was indirectly obtained by calculating the difference. Fig. 2a shows the FTIR spectra for SB and STA. The main changes highlighted in the FTIR spectrum for SB in comparison with STA are: (1) the appearance of a band at 2640 cm^{-1}, which can be attributed to the stretching of hydrogen bonding present in the dimmer of carboxylic acid; (2) a strong band at 1717 cm^{-1}, which can be attributed to the stretching of conjugated carbonyl ester; (3) a band at 1491 cm^{-1}, which can be attributed to the stretching of C=C bonds in the aromatic ring of the trimellitate moiety; (4) a band at 1281 cm^{-1}, which can be attributed to the C—O stretching of esters of aromatic acids; and (5) a band at 754 cm^{-1}, which can be attributed to C—H out-of-plane bending for the 1,2,4-substituted benzenoid compound (Pavia et al., 2009). These changes confirmed the introduction of the trimellitate group to the SB. Similar band assignments were reported by Saikia et al. (1993), who esterified different cellulose pulps with TA.

Fig. 2b shows FTIR spectra for STA and STA-loaded with Co^{2+}, Cu^{2+}, and Ni^{2+}. The adsorption of metal ions on STA was characterized by the two new bands arising at 1592 and 1552 cm^{-1}, which can be attributed to asymmetric stretching of different carboxylate groups and indicate the complete deprotonation of carboxylic acid
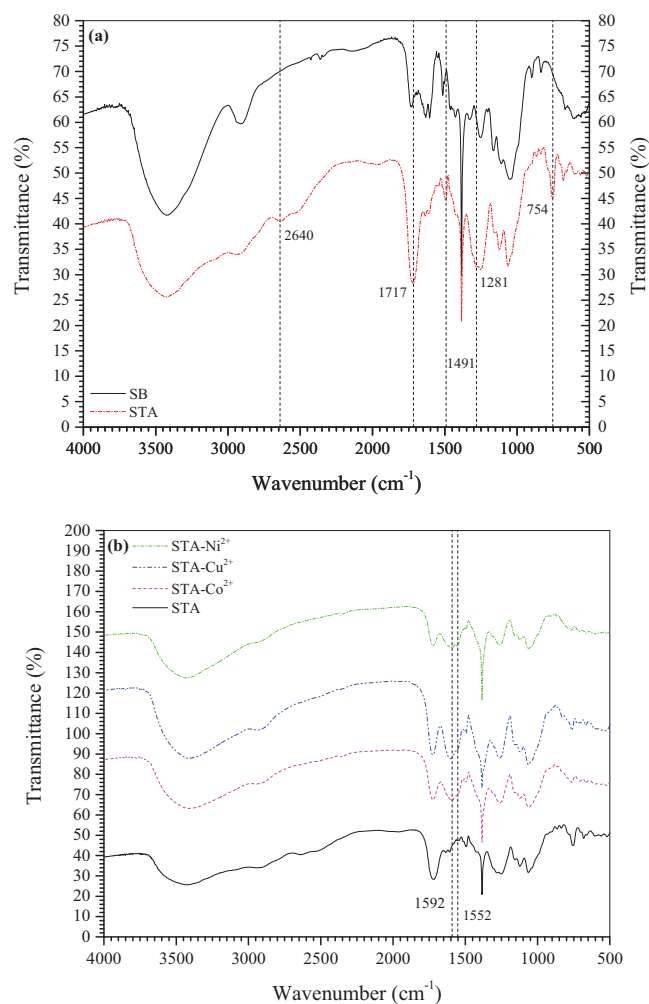

Fig. 2. FTIR spectra of (a) SB and STA and (b) STA and STA-loaded with Co^{2+}, Cu^{2+}, and Ni^{2+} (transmittances of STA–Co^{2+}, STA–Cu^{2+}, and STA–Ni^{2+} spectra were shifted by 30, 60 and 90%).

groups during the adsorption process. These bands prove the participation of all carboxylate groups during the adsorption of metal ions, as suggested in the adsorption mechanism proposed in Fig. 1b (Łyszczek, 2007). According to Łyszczek (2007), the splitting of the carboxylate band is suggestive of the presence of a non-equivalence of carboxylate groups. The similarities between the spectra of STA-loaded with Co^{2+}, Cu^{2+}, and Ni^{2+} suggest similar metal coordination through the carboxylate groups.

3.1.3. Thermogravimetric analysis (TGA)

TGA data for the thermal decomposition of SB and STA are presented in Table 2. TGA and DTG curves are shown in Supplementary Fig. 1. As can be seen in Supplementary Fig. 1 and Table 2, the first weight loss occurred at $T_{m,1}$ = 53–58 °C for SB and STA, which can be attributed to the vaporization of bound water. The TGA curve of SB exhibited two main decomposition events. The DTG peaks at $T_{m,2}$ = 322 °C and $T_{m,3}$ = 368.5 °C for SB are attributed to hemicelluloses and cellulose decomposition, which break down faster than lignin, yielding volatile compounds (Varhegyi et al., 1989). The thermal decomposition of lignin follows a slow charring process over a broad temperature range above 400 °C (flat DTG portion) and does not exhibit a DTG peak (Varhegyi et al., 1989). The TGA curve of STA also exhibited two main decomposition events, but they were better defined in comparison with SB. Compared to SB, STA showed a lower thermal stability, as indicated by the lower initial
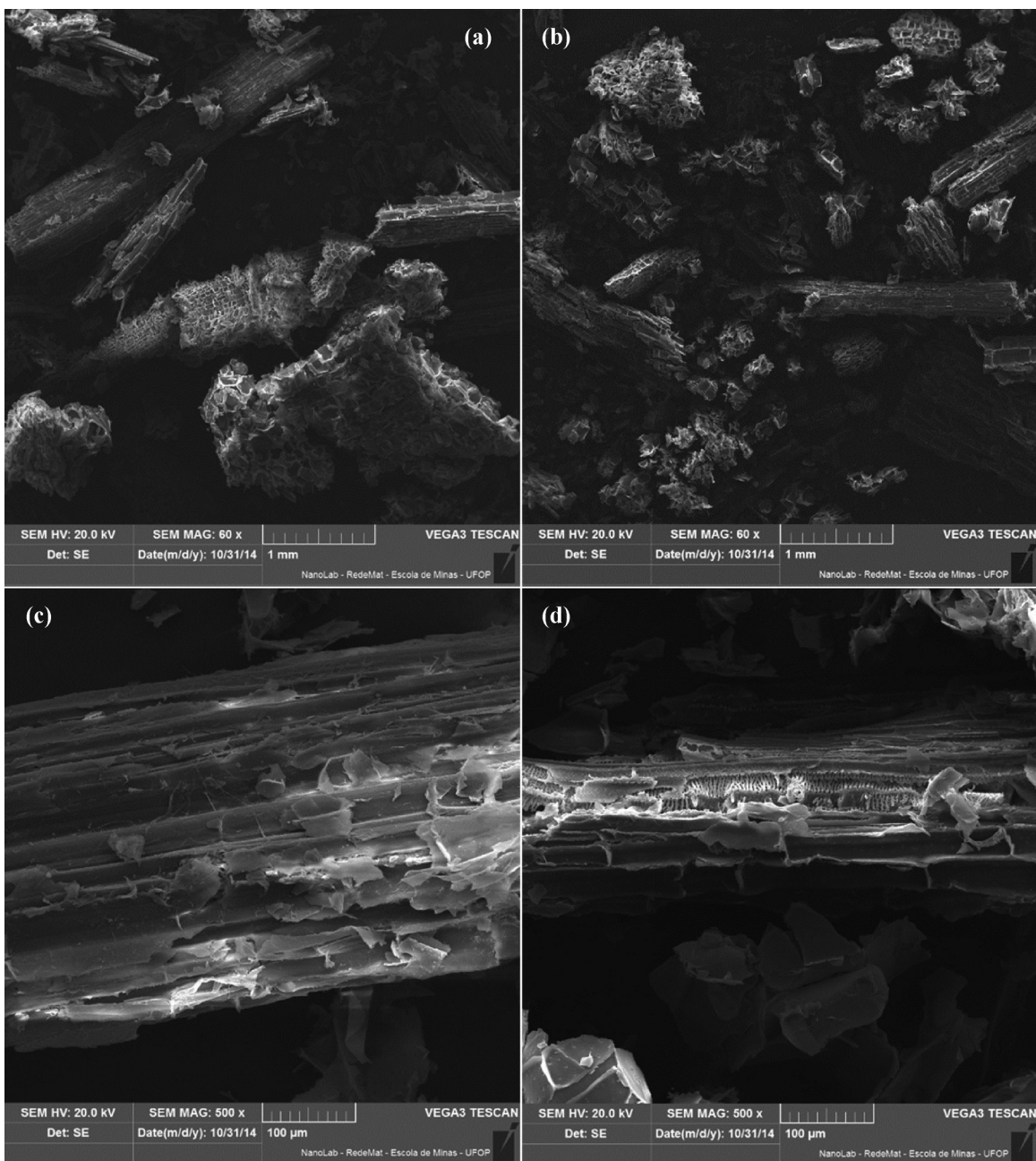
Fig. 3. SEM images of SB (a and c) and STA (b and d) at 60 and 500 fold magnification.

Table 2
TGA data for the thermal decomposition of SB and STA.

Parameters[a]	SB	STA
$T_{i,1}$ (°C)	35.3	36.4
$T_{m,1}$ (°C)	53.0	58.0
ΔW_1 (%)	5.45	4.98
$T_{i,2}$ (°C)	202.3	134.0
$T_{m,2}$ (°C)	322.0	242.4
ΔW_2 (%)	33.85	48.68
$T_{i,3}$ (°C)	340.0	293.4
$T_{m,3}$ (°C)	368.5	324.3
ΔW_3 (%)	44.36	24.11
$T_{i,4}$ (°C)	404.0	363.8
$T_{m,4}$ (°C)	–	–
ΔW_4 (%)	10.46	8.30

[a] T_i: initial decomposition temperature. T_D: maximum decomposition temperature (DTG peak), and ΔW: weight loss in the decomposition event.

decomposition temperatures (T_i). The DTG peaks at $T_{m,2}$ and $T_{m,3}$ for STA were also shifted to lower temperatures in comparison with $T_{m,2}$ and $T_{m,3}$ for SB. The second weight loss for STA also increased in relation to SB, whereas the third weight loss for STA was smaller than SB. These results demonstrate that the esterification of SB with TA decreases its thermal stability. Similar trends were observed by Nada and Hassan (2006) and Ferreira et al. (2015), who studied the succinylation ($T_{m,2}$ and $T_{m,3}$ were 319 and 417 °C, respectively) and malonylation ($T_{m,2}$ and $T_{m,3}$ were 206.9 and 350.5 °C, respectively) of SB.

3.1.4. Point of zero charge (PZC)

The PZC was used to assess the surface properties of the STA adsorbent. The pH necessary to give a net zero surface charge can be related to the acidity constant (K_a) of an adsorbent material (Noh and Schwarz, 1990). Therefore, the surface of an adsorbent has a net

positive charge at pH < PZC, whereas at pH > PZC, it has a net negative surface charge. The PZC of the STA adsorbent was found to be 3.16 ± 0.07. The pK_a values of the trimellitic acid corresponding to position of carboxyl groups 1, 2, and 4 are 2.52, 3.84, and 5.20 (Fig. 1), respectively (Braude and Nachod, 1955). The comparison between the PZC of STA and the pK_a values of trimellitic acid suggests that electronic effects provided by the presence of the ester linkage between the trimellitate and the hydroxyl groups of SB influence the acidity of the remaining carboxyl groups. The PZC value of STA suggests that the adsorption of metal ions will take place at pH ≥ 3.16.

3.1.5. Scanning electron microscopy (SEM)

SEM was used to assess the morphological and surface features of the SB and STA adsorbent. SEM images were also used to assess the changes in the surface of SB after chemical modification with TA. Fig. 3 shows SEM images of SB and STA at 60 (a and b) and at 500-fold (c and d) magnification. As can be seen in Fig. 3a, the SB (the 60-mesh fraction) is composed of a variety of particles of different elements with different sizes and morphologies. The morphology of the SB particles (Fig. 3a) suggests that the milling process partially disintegrated the fibers, as the presence of damaged fibrous and pith material is noticeable. As can be seen in Fig. 3b, after chemical modification of SB with TA, the particle size was apparently reduced. Disintegration of some particles may have been caused by swelling and agitation during the chemical modification. In Fig. 3c, it is noticeable that the surface of the fibers was exposed during the milling process and its open interior can be seen. After chemical modification, the fibers were more exposed and the presence of porous elements can be seen, as shown in Fig. 3d. The exposure of these pores may increase the diffusion of metal ions into the fibers, which may increase the adsorption capacity of the STA adsorbent.

3.1.6. Energy dispersive X-ray (EDX) spectroscopy

EDX spectroscopy was used to map the surface of the STA adsorbent in order to assess the adsorption sites containing adsorbed metal ions and their distribution along the surface of the adsorbent. Supplementary Figs. 2a–c show the distribution of Co^{2+}, Cu^{2+}, and Ni^{2+} on the surface of the STA adsorbent. As can be seen in Supplementary Figs. 2a–c, a heterogeneous distribution of Co^{2+}, Cu^{2+}, and Ni^{2+} was observed on the surface of STA adsorbent with a higher concentration of metal ions at some regions. The Langmuir and Sips models provides better fits for the adsorption of Co^{2+}, Cu^{2+}, and Ni^{2+} on the STA adsorbent, which suggests a homogeneous adsorption layer on the STA surface. However, in Supplementary Figs. 2a–c, it seems that there are some preferred adsorption sites. Nevertheless, the Langmuir model would be representative, considering that there is no evidence of multilayer formation, only the presence of sparsely and preferential adsorption sites. Similar results were reported by Vieira and Beppu (2006) for the adsorption of Hg^{2+} on raw and crosslinked chitosan films.

3.2. Adsorption experiments

3.2.1. Effect of solution pH on metal ion adsorption

The effect of the solution pH on metal ion adsorption was evaluated at 25 °C with a 0.79 mmol/L metal ion solution, 130 rpm, 0.2 g/L adsorbent, as well as 180, 250, and 75 min equilibrium time (t_e) (based on kinetic data) for Co^{2+}, Cu^{2+}, and Ni^{2+}, respectively. Fig. 4 shows the equilibrium adsorption capacity (q_e) of Co^{2+}, Cu^{2+}, and Ni^{2+} on the STA adsorbent as a function of the solution pH from 2.0 to 5.75. The uptake of metal ions from aqueous solution hardly depends on the solution pH, as the pH affects both the surface charge of the adsorbent and the form of the metallic ions in the aqueous solution (Karnitz et al., 2009; Srivastava et al., 2009). The surface charge of an adsorbent in aqueous solution is
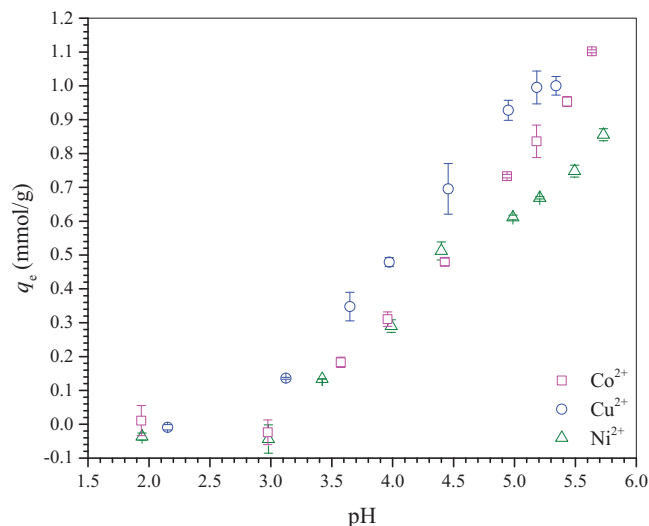

Fig. 4. Effect of pH on adsorption of Co^{2+}, Cu^{2+}, and Ni^{2+} on the STA (0.79 mmol/L M^{2+}, 130 rpm, 25 °C, 0.2 g/L STA and 180, 250, and 75 min of shaking for Co^{2+}, Cu^{2+}, and Ni^{2+}, respectively).

related to its PZC value. The PZC of STA was 3.16. Consequently, the adsorption of metal ions was favored at pH > PZC, where the STA surface is negatively charged, owing to deprotonation of the carboxylate groups of the trimellitate moiety that is grafted on SB. Fig. 4 shows that the q_e increased as the solution pH increased, and a plateau was not reached. At low pH values (pH < 3), the carboxylate groups on the STA surface were protonated and the adsorption of metal ions did not take place. From pH values slightly higher than PZC, the adsorption begins to take place as a consequence of strong attractions between the negatively charged carboxylate groups containing unshared electron pairs on the STA surface and cationic metal ions in solution. Adsorption at pH values higher than 5.75 was not studied, as the formation of metal-hydrolyzed species $[M(OH)^+]$ and the precipitation of metal ions $[M(OH)_{2(s)}]$ may occur. Thus, the pH values of 5.5 for Cu^{2+} and 5.75 for Co^{2+} and Ni^{2+} were considered as optimum pH values for the subsequent adsorption studies.

3.2.2. Adsorption kinetics

The adsorption kinetics represent one of the most important parameters for designing a wastewater treatment system with a batch adsorption process (Ferreira et al., 2015). Pseudo-first- and second-order kinetic models were used to model the adsorption rate of metal ions on the STA adsorbent at pH 5.5 for Cu^{2+} and 5.75 for Co^{2+} and Ni^{2+} at 25 °C, 130 rpm, 0.79 mmol/L M^{2+}, and 0.2 g/L adsorbent.

The pseudo-first-order kinetic model of Lagergren (1898) defines the adsorption rate in terms of adsorption capacity as follows in Eq. (6):

$$\frac{dq_t}{dt} = k_1 (q_e - q_t) \tag{6}$$

where q_e and q_t (mmol/g) are the adsorption capacities at equilibrium t_e and time t (min), respectively, and k_1 (min^{-1}) is the pseudo-first-order rate constant. Rearranging and integrating Eq. (6) using the boundary conditions $q_t = 0$ at $t = 0$ and $q_t = q_t$ at $t = t$, gives Eq. (7):

$$q_t = q_e (1 - \exp^{-k_1 t}) \tag{7}$$

The pseudo-second-order kinetic model of Ho and McKay (1998) also defines the adsorption rate in terms of adsorption capacity; however, it assumes that the rate-limiting step may be chemical adsorption involving valency forces through sharing or exchange of

Table 3
Results of nonlinear regression analysis of the experimental data for adsorption of metal ions on STA (0.79 mmol/L M^{2+}, 25 °C, 130 rpm, 0.2 g/L STA).

| Parameters	Co^{2+}	Cu^{2+}	Ni^{2+}
pH	5.75	5.5	5.75
t_e (min)	180	250	75
$q_{e,exp}$ (mmol/g)	1.168 ± 0.026	0.979 ± 0.011	0.849 ± 0.020
Pseudo–first–order			
$q_{e,est}$ (mmol/g)	1.062 ± 0.047	0.808 ± 0.047	0.782 ± 0.03
k_1 (min^{-1})	$(7.22 \pm 1.16) \times 10^{-2}$	$(7.87 \pm 1.69) \times 10^{-2}$	$(1.76 \pm 0.33) \times 10^{-1}$
R^2	0.8816	0.7736	0.8419
χ^2_{red}	0.0179	0.0231	0.0108
Pseudo–second–order			
$q_{e,est}$ (mmol/g)	1.153 ± 0.035	0.979 ± 0.051	0.849 ± 0.020
k_2 (g/mmol min)	$(8.74 \pm 1.30) \times 10^{-2}$	$(7.80 \pm 1.93) \times 10^{-2}$	$(2.84 \pm 0.38) \times 10^{-1}$
R^2	0.9580	0.8694	0.9617
χ^2_{red}	0.0064	0.0133	0.0026
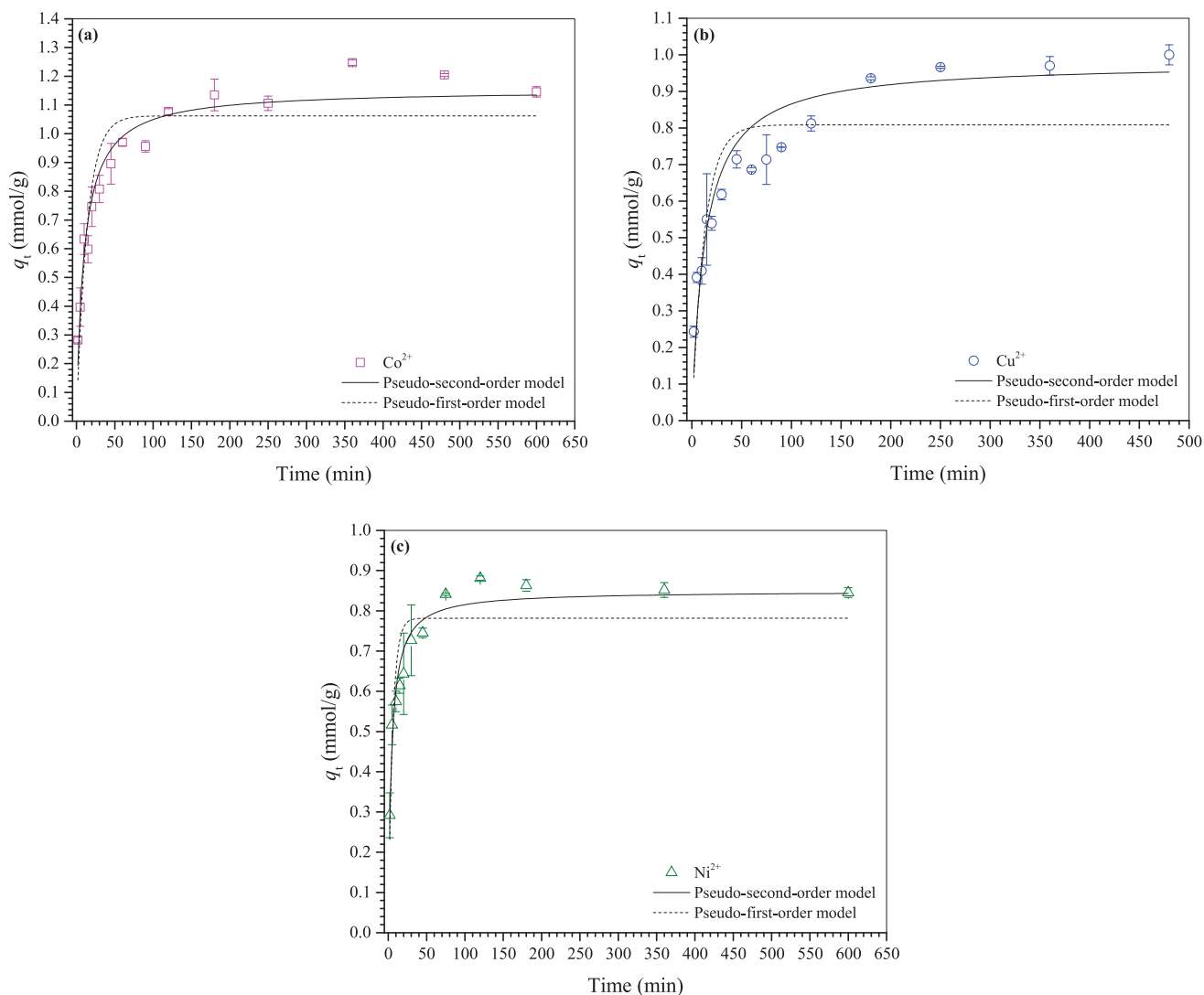
Fig. 5. Adsorption kinetics of (a) Co^{2+}, (b) Cu^{2+}, and (c) Ni^{2+} on the STA at pH 5.75 for Co^{2+} and Ni^{2+} and 5.5 for Cu^{2+}, 0.79 mmol/L M^{2+}, 25 °C, 130 rpm, and 0.2 g/L STA.

electrons between adsorbate and adsorbent (Ho and McKay, 1999). It can be expressed as Eq. (8):

$$\frac{dq_t}{dt} = k_2(q_e - q_t)^2 \tag{8}$$

where q_e and q_t (mmol/g) are the adsorption capacities at equilibrium t_e and time t (min), respectively, and k_2 (g/mmol min) is the pseudo-second-order rate constant. Rearranging and integrat-

ing Eq. (8) using boundary conditions $q_t = 0$ at $t = 0$ and $q_t = q_t$ at $t = t$, gives Eq. (9):

$$q_t = \frac{k_2 q_e^2 t}{1 + k_2 q_e t} \tag{9}$$

The results were obtained by nonlinear regression analysis of pseudo-first- and second-order kinetic models using the

Microcal OriginPro 2015^{TM} set to use the iteration algorithm as Levenberg–Marquardt and the weight method as the statistical [Eq. (10)]. In this procedure the weights are used to minimize the χ^2 [Eq. (11)] in order to obtain the best fit. Both the coefficient of determination (R^2) and reduced χ^2 [Eq. (12)] were used to measure the quality of the nonlinear regression analysis and define the best model describing the adsorption.

$$w_i = \frac{1}{y_i} \tag{10}$$

where w_i is the weighting coefficient and y_i is the experimental data point.

$$\chi^2 = \sum_{i=1}^{n} w_i \left(y_i - \hat{y}_i \right)^2 \tag{11}$$

where $\hat{y}_i$ is the theoretical data point calculated by the model.

$$\chi^2_{red} = \frac{\chi^2}{\upsilon} \tag{12}$$

where $\chi^2{}_{red}$ is the reduced chi-square value and υ is the number of degrees of freedom.

Table 3 shows the results of nonlinear regression analysis of kinetic data. Plots of q_t against t are shown in Fig. 5a–c for the kinetic data and nonlinear fits for pseudo-first- and second-order kinetic models (experimental kinetic data available in Supplementary Table 1). As can be seen in Table 3, both values of R^2 and χ^2 obtained from fitting the experimental data to the pseudo-second-order model were higher and lower in comparison with pseudo-first-order model, respectively. Furthermore, when the experimental equilibrium adsorption capacity ($q_{e,exp}$) is compared to the estimated equilibrium adsorption capacity ($q_{e,est}$), it is noticeable that the values provided by the pseudo-second-order model were closer than those provided by the pseudo-first-order model, indicating that the pseudo-second-order model better describes the adsorption kinetics of Co^{2+}, Cu^{2+}, and Ni^{2+} on the STA. The ratios of $k_{2,Co/Cu}$, $k_{2,Ni/Co}$ and $k_{2,Ni/Cu}$ are 1.12, 9.72, and 10.9, respectively. This means that Ni^{2+} is adsorbed by STA almost 10 times faster than Co^{2+} and Cu^{2+}. This finding indicates that it would be possible to make a kinetic separation of Ni^{2+} with respect to Co^{2+} and Cu^{2+} in a multicomponent ion solution if a low agitation time is used. For example, the separation of Co^{2+}, Cu^{2+}, and Ni^{2+} from aqueous solutions is often required in hydrometallurgy processing (Pośpiech and Walkowiak, 2007) and industrial wastes (Yavuz et al., 2003).

3.2.3. Adsorption isotherms

Adsorption isotherms describe how various types of pollutants interact with the adsorbent materials, and, therefore, are critical in the elucidation of the adsorption mechanism, and in determining the equilibrium adsorption capacity and their influence on the surface properties on adsorption. Thus, they are crucial in the design of adsorption systems (Ferreira et al., 2015; Foo and Hameed, 2010). Adsorption of Co^{2+}, Cu^{2+}, and Ni^{2+} on the STA was studied in mono- and bi-component aqueous solutions at 25 °C, 130 rpm, 0.2 g/L STA, 0.05–1.12 mmol/L M^{2+}, and an equilibrium time of 300 min (based on kinetic data of Section 3.2.2).

3.2.3.1. Monocomponent adsorption.

Monocomponent isotherm equations of Langmuir, Freundlich, Sips, and Redlich–Peterson (R–P) have been used to describe the equilibrium characteristics of adsorption (Srivastava et al., 2006).

The Freundlich isotherm (Freundlich, 1906) derivation assumes adsorption on a heterogeneous surface with a non-uniform distribution of heat of adsorption over the surface. Whereas, the Langmuir isotherm (Langmuir, 1918) assumes adsorption on a homogeneous surface with the adsorption sites having the same energy or equal affinity for the adsorbate (Srivastava et al., 2006).

The Sips (Langmuir–Freundlich) isotherm (Sips, 1948) can be described as follows in Eq. (13):

$$q_e = Q_{max} \frac{(bC_e)^{1/n}}{1 + (bC_e)^{1/n}} \tag{13}$$

where q_e (mmol/g) is the equilibrium adsorption capacity, C_e (mmol/L) is the metal ion equilibrium concentration in the solution, Q_{max} is the maximum adsorption capacity (mmol/g), b (L/mmol) is the Sips constant related to the energy of adsorption, and n is the parameter characterizing the heterogeneity of adsorption system. If parameter n is unity, the Sips isotherm [Eq. (13)] reduces to the Langmuir isotherm [Eq. (16)] for ideal surfaces.

The R–P isotherm (Redlich and Peterson, 1959) can be described as follows in Eq. (14):

$$q_e = \frac{K_R C_e}{1 + a_R C_e^{\beta}} \tag{14}$$

where K_R (L/g) and a_R (L/mmol) are the R–P isotherm constants and β is the R–P isotherm exponent, which is dimensionless and lies between 0 and 1.

For high concentrations, the R–P isotherm [Eq. (14)] reduces to the Freundlich isotherm as follows in Eq. (15):

$$q_e = K_F C_e^{1/n} \tag{15}$$

where $K_F = K_R/a_R$ is the Freundlich constant [(mmol/g)(L/mmol)$^{1/n}$] and n is the heterogeneity factor ($1/n = 1 - \beta$) (Srivastava et al., 2006).

For $\beta = 1$, Eq. (14) reduces to the Langmuir isotherm as follows in Eq. (16):

$$q_e = \frac{Q_{max} b C_e}{1 + b C_e} \tag{16}$$

where b (L/mmol) is the Langmuir constant related to the energy of adsorption and $Q_{max} = K_R/a_R$ is the maximum adsorption capacity (mmol/g).

For $\beta = 0$, Eq. (14) reduces to the Henry's equation as follows in Eq. (17):

$$q_e = \frac{K_R C_e}{1 + a_R} \tag{17}$$

The change in free energy of adsorption of the system ($\Delta_{ads}G°$) can be calculated as follows in Eq. (18) (Liu, 2009):

$$\Delta_{ads}G° = -RT\ln K_a \tag{18}$$

where K_a is the thermodynamic equilibrium constant, T (K) is the absolute temperature, and R is the ideal gas constant (8.314 J/K mol).

The thermodynamic equilibrium constant can be calculated from Langmuir constant, b, as follows in Eq. (19) (Liu, 2009):

$$K_a = \left[\frac{b}{\gamma_e}(1 \text{ mol}/L) \right] \tag{19}$$

where γ_e is the activity coefficient in the equilibrium (dimensionless) at 25 °C.

When the adsorbate is a metal ion, the activity coefficient is strongly affected and it rapidly decreases as the ionic strength increases. For this reason, it is necessary to correct the activity coefficient for each adsorption system studied using the extended

Debye–Hückel law [Eq. (20)] to provide a correct calculation of $\Delta_{ads}G^{\circ}$, as postulated by Liu (2009).

$$\log \gamma_e = \frac{-0.509 z^2 \sqrt{I_e}}{1 + \left(\alpha \sqrt{I_e/305}\right)} \tag{20}$$

where z is the charge of the ion, I_e (mol/L) is the ionic strength in the equilibrium and α (pm) is the ion size considered as 600 pm for Co^{2+}, Cu^{2+}, and Ni^{2+} (Harris, 2010). The ionic strength was calculated using the first equilibrium concentration data point of the plateau of the mono- and bi-component adsorption isotherms.

Monocomponent isotherm model parameters were found using Microcal OriginPro™ 2015 software by minimizing χ^2 as presented in Section 3.2.2.

The equilibrium monocomponent adsorption isotherms for the adsorption of Co^{2+}, Cu^{2+}, and Ni^{2+} on the STA at 25 °C, 130 rpm, and 0.2 g/L STA are shown in Fig. 6a–c. The monocomponent adsorption was investigated at pH 5.75 for Co^{2+} and Ni^{2+} and 5.5 for Cu^{2+}. Table 4 presents the results of modeling the experimental adsorption data through nonlinear regression analysis for the four monocomponent isotherms (Langmuir, Freundlich, Sips, and R–P) (experimental equilibrium data available in Supplementary Table 2). Table 4 shows that considering the values of $Q_{max,exp}$, R^2, and χ^2 the adsorption of Co^{2+} was best described by the Sips isotherm, whereas the adsorption of Cu^{2+} and Ni^{2+} was best described by the Langmuir isotherm. In fact, the STA presents a heterogeneous surface where carboxylic acid groups compose the majority of the chemical functional groups. However, there are other functional groups, such as phenolic and carbonyl groups, in lignin. Thus, the surface of STA is not composed of adsorption sites with equal energy or affinity to the adsorbate. Therefore, the adsorption system cannot be considered as fully Langmuirian. In other words, although the Langmuir model failed to describe the adsorption system to a certain degree, the use of estimated Langmuir constants for comparison of the STA performance is essential. The Sips isotherm constant, n, can be used as an estimation of the heterogeneity of the adsorption system, as this isotherm is a combination of Langmuir and Freundlich isotherms. The values of n from the Sips isotherm for the adsorption of Co^{2+}, Cu^{2+}, and Ni^{2+} were reasonably close to unity. This suggests that the adsorption system is more Langmuirian than Freundlichian. The maximum metal ion adsorption capacity of the STA adsorbent presented the following order $Ni^{2+} > Cu^{2+} > Co^{2+}$. Coordination numbers (CNs) higher than unity indicate that more than one carboxylate group is being used to adsorb a metal ion. As the monocomponent adsorption systems were best described by the Langmuir theory, it was decided that the modified Langmuir models would be used to analyze the bicomponent adsorption data, which are presented in the next Section.

The difference between physisorption and chemisorption lies in the magnitude of changes in enthalpy and free energy. For physisorption and chemisorption, the values of $\Delta_{ads}G^{\circ}$ are in the range from 0 to −20 kJ/mol and −80 to −200 kJ/mol, respectively (Húmpola et al., 2013). The values of $\Delta_{ads}G^{\circ}$ for adsorption of Co^{2+}, Cu^{2+}, and Ni^{2+} on the STA are in the range from −22.8 to −25.2 kJ/mol, which is slightly higher than physisorption and lower than chemisorption, suggesting that a mixed mechanism may be controlling the uptake of metal ions on STA. Further evidence that can be used to understand the mechanism controlling the uptake of Co^{2+}, Cu^{2+}, and Ni^{2+} on the STA is the shift of the carboxylate band in the FTIR spectra, which indicates the complete deprotonation of carboxylic acid groups during the adsorption process. This shift in the carboxylate band in the FTIR spectra also indicates that valence electrons from carboxylate groups are being used to complex metal ions. However, considering the magnitude of $\Delta_{ads}G^{\circ}$, it is possible to suggest that fairly weak bond was formed between the carboxy-

late groups and metal ions studied. This finding will be confirmed from desorption data, which are presented in Section 3.3.

3.2.3.2. Multicomponent adsorption.

Three bicomponent adsorption systems Co^{2+}–Cu^{2+}, Co^{2+}–Ni^{2+}, and Cu^{2+}–Ni^{2+} were modeled using three predictive models: (1) the non-modified competitive Langmuir model, (2) the Jain and Snoeyink (J–S) modified extended Langmuir model, and (3) P-factor and one correlative or semi-predictive: modified extended Langmuir model (interaction factor). The binary mixtures of metal ions were equimolar ($C_i = C_j$) with concentrations varying from 0.05 to 1.12 mmol/L.

The non-modified competitive Langmuir model (Butler and Ockrent, 1930) is an extension of the Langmuir isotherm model for a component i in a system with N components and it can be described as follows in Eq. (21):

$$q_{e,i} = \frac{Q_{max,i} b_i C_{e,i}}{1 + \sum_{j=1}^{N} b_j C_{e,j}} \tag{21}$$

where $Q_{max,i}$ and b are the Langmuir constants derived from monocomponent Langmuir isotherm for components i and j.

The J–S modified extended Langmuir model (Jain and Snoeyink, 1973) is a bicomponent adsorption model developed to model non-ideal adsorption systems. Contrary to the non-modified extended Langmuir model, the J–S model accounts for competitive adsorption. The J–S model can be described as follows in Eqs. (22) and (23):

$$q_{e,i} = \frac{\left(Q_{max,i} - Q_{max,j}\right) b_i C_{e,i}}{1 + b_i C_{e,i}} + \frac{Q_{max,j} b_i C_{e,i}}{1 + b_i C_{e,i} + b_j C_{e,j}} \tag{22}$$

$$q_{e,j} = \frac{Q_{max,j} b_j C_{e,j}}{1 + b_i C_{e,i} + b_j C_{e,j}} \tag{23}$$

where Q_{max} and b are the Langmuir constants derived from monocomponent Langmuir isotherm for components i and j. The first term $(Q_{max,i} - Q_{max,j})$ on the left-hand side of Eq. (22) refers to the amount of solute i adsorbed without competition from solute j; whereas, the second term on the right-hand side of Eq. (22) refers to the amount of solute i adsorbed in competition with solute j.

The P-factor is a correlative technique developed by McKay and Al Duri (1987). This model assumes a Langmuir isotherm and can be described as follows in Eq. (24):

$$q_{e,i,multi} = \frac{1}{P_i} \left(\frac{K_{L,i} C_{e,i,multi}}{1 + a_{L,i} C_{e,i,multi}} \right) \tag{24}$$

where P_i is a "lumped" capacity factor and can be defined as follows in Eq. (25):

$$P_i = \frac{(K_{L,i}/a_{L,i})_{mono}}{(K_{L,i}/a_{L,i})_{multi}} = \frac{Q_{max,mono}}{Q_{max,multi}} \tag{25}$$

where $(K_{L,i}/a_{L,i})_{mono}$ and $(K_{L,i}/a_{L,i})_{multi}$ are the maximum adsorption capacities for component i in a monocomponent and multicomponent system, respectively.

The modified extended competitive Langmuir model is also an extension of the Langmuir isotherm model for a component i in a system with N components that incorporates an interaction factor, η [Eq. (26)] (Mathews and Weber, 1980).

$$q_{e,i} = \frac{Q_{max,i} b_i \left(C_{e,i}/\eta_i\right)}{1 + \sum_{j=1}^{N} b_j \left(C_{e,j}/\eta_j\right)} \tag{26}$$

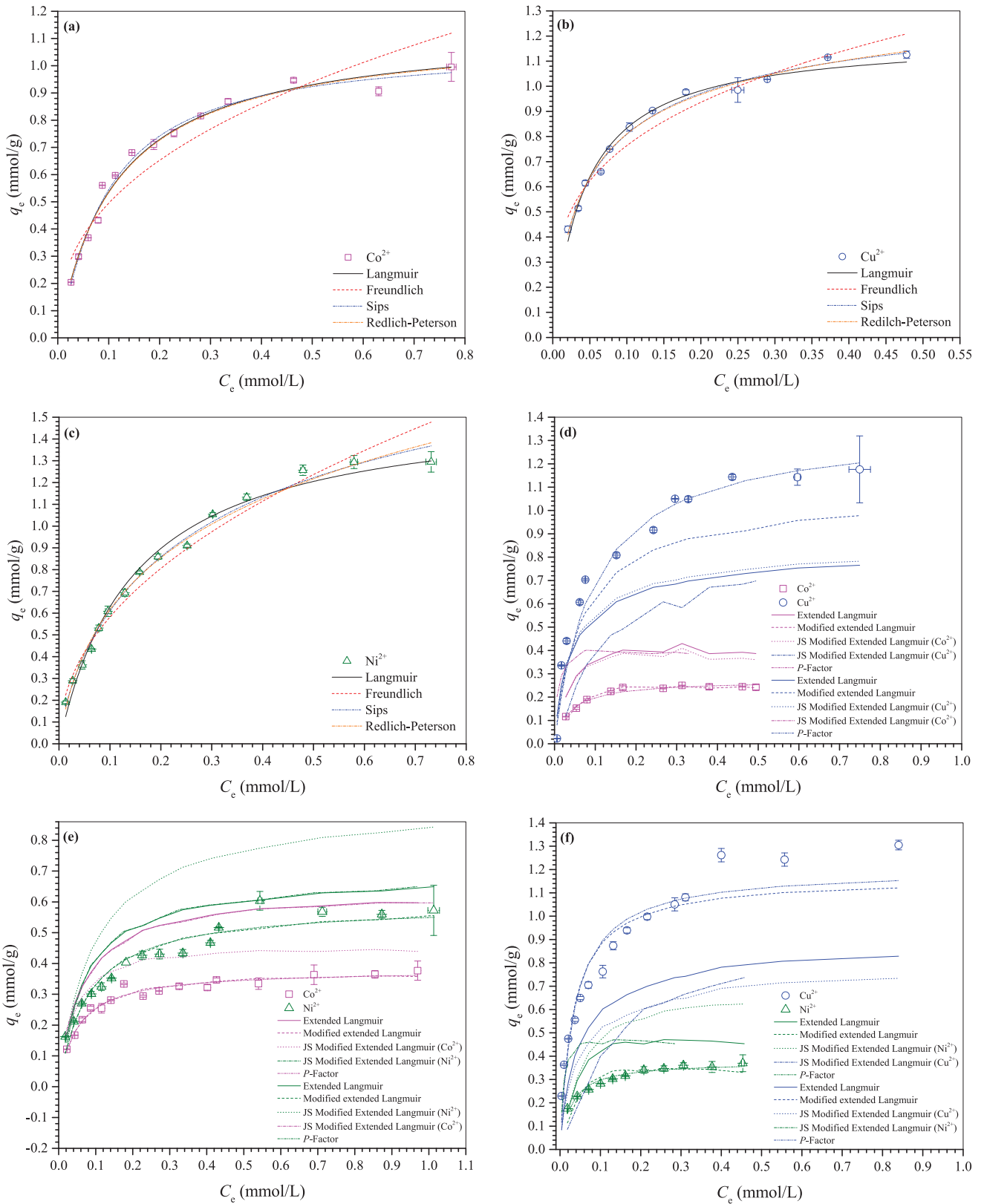**Fig. 6.** Equilibrium adsorption isotherms for monocomponent adsorption of (a) Co^{2+}, (b) Cu^{2+}, and (c) Ni^{2+} on the STA at 25 °C, pH 5.75 for Co^{2+} (180 min) and Ni^{2+} (75 min), and 5.5 for Cu^{2+} (250 min), 130 rpm, 0.2 g/L STA and bicomponent adsorption of (d) Co^{2+}–Cu^{2+} (250 min), (e) Co^{2+}–Ni^{2+} (180 min), and (f) Cu^{2+}–Ni^{2+} (250 min) at pH 5.5.

Table 4
Results of modeling the equilibrium adsorption isotherm with monocomponent isotherm models (25 °C, 130 rpm and 0.2 g/L STA).

Monocomponent				
Isotherm model	Parameters	Co^{2+}	Cu^{2+}	Ni^{2+}
	$Q_{max,exp}$ (mmol/g)	0.950 ± 0.026	1.121 ± 0.005	1.295 ± 0.000
	pH	5.75	5.5	5.75
	t_e (min)	180	250	75
	CN	3.98	3.37	2.92
	I_e (mol/L)	0.0515	0.0523	0.0521
	γ_e	0.886	0.886	0.886
Langmuir	$Q_{max,est}$ (mmol/g)	1.140 ± 0.034	1.197 ± 0.028	1.563 ± 0.066
	b (L/mmol)	8.87 ± 0.67	22.95 ± 1.76	6.73 ± 0.65
	R^2	0.9864	0.9804	0.9835
	χ^2_{red}	0.0018	0.0015	0.0038
	$\Delta_{ads}G°$	-22.83 ± 1.72	-25.19 ± 1.93	-22.15 ± 2.14
Freundlich	K [mmol/g/(L/mmol)$^{1/n}$]	1.241 ± 0.082	1.501 ± 0.064	1.711 ± 0.064
	n	2.50 ± 0.23	3.41 ± 0.23	2.14 ± 0.10
	R^2	0.9083	0.9553	0.9772
	χ^2_{red}	0.0123	0.0035	0.0052
Sips	$Q_{max,est}$ (mmol/g)	1.067 ± 0.052	1.379 ± 0.105	2.153 ± 0.262
	b (L/mmol)	10.36 ± 1.17	15.98 ± 3.66	2.88 ± 0.96
	n	$0.89 \pm n0.08$	1.34 ± 0.16	1.34 ± 0.10
	R^2	0.9874	0.9884	0.9931
	χ^2_{red}	0.0017	0.0009	0.0016
Redlich–Peterson	K_R (L/g)	10.03 ± 1.15	37.81 ± 6.41	16.84 ± 3.22
	a_R (L/mmol)	8.82 ± 0.95	28.78 ± 4.20	10.03 ± 1.89
	b	1.00 ± 0.07	0.90 ± 0.04	0.76 ± 0.06
	R^2	0.9851	0.9869	0.99
	χ^2_{red}	0.002	0.001	0.0023

where η_i and η_j are interaction factors that can be estimated from competitive adsorption data.

The predictive multicomponent adsorption isotherms were fed with monocomponent parameters obtained from nonlinear regression analysis of the Langmuir model, as presented in Table 4. The Microsoft Excel™ 365 software for Windows™ was used

to calculate R^2 and χ^2 using equilibrium concentrations for each metal ion. The interaction factor of the semi-predictive model (fed with monocomponent parameters from Langmuir model) was obtained by minimizing χ^2 using Microcal OriginPro™ 2015 software as described in Section 3.2.2. The Langmuir isotherm was also used to estimate multicomponent isotherms in order

Table 5
Results of equilibrium adsorption isotherm modeling, using multicomponent isotherm models (25 °C, 130 rpm and 0.2 g/L STA).

Bicomponent systems							
Isotherm model	Parameters	Co–Cu	Cu–Co	Co–Ni	Ni–Co	Cu–Ni	Ni–Cu
	$Q_{max,exp,i}$ (mmol/g)	0.246 ± 0.003	1.154 ± 0.019	0.368 ± 0.007	0.576 ± 0.019	1.283 ± 0.022	0.365 ± 0.007
	$Q_{max,exp,i+j}$ (mmol/g)	1.400 ± 0.019		0.944 ± 0.021		1.658 ± 0.023	
	$Q_{max,exp,i,multi}/Q_{max,exp,mono}$	0.259	1.030	0.388	0.445	1.145	0.282
	pH	5.5	5.5	5.5	5.5	5.5	5.5
	$t_{e,mono}$ (min)	250	250	180	180	250	250
	I_e (mol/L)	0.0531		0.0554		0.0535	
	γ_e	0.886		0.886		0.886	
Langmuir	$Q_{max,est}$ (mmol/g)	0.272 ± 0.006	1.361 ± 0.128	0.380 ± 0.008	0.593 ± 0.025	1.165 ± 0.067	0.376 ± 0.009
	b (L/mmol)	27.47 ± 2.78	10.47 ± 2.71	20.32 ± 1.70	12.70 ± 1.82	30.19 ± 6.20	38.51 ± 4.52
	R^2	0.9702	0.9588	0.9732	0.9365	0.9213	0.9548
	χ^2_{red}	0.0004	0.0262	0.0007	0.0035	0.0139	0.0007
	$\Delta_{ads}G°$	-32.61 ± 3.30	-30.36 ± 2.32	-24.89 ± 2.08	-23.73 ± 3.39	-25.87 ± 5.31	-26.48 ± 3.11
Non-modified extended Langmuir	R^2	0.4237	0.7859	0.5822	0.9579	0.8766	0.8562
	χ^2_{red}	0.1128	0.0957	0.1173	0.0014	0.1006	0.0046
Modified extended Langmuir	η_i	2.178 ± 0.089	1.571 ± 0.517	1.378 ± 0.099	1.366 ± 0.161	0.735 ± 0.151	1.440 ± 0.192
	η_j	1.149 ± 0.070	6.000 ± 7.869	0.539 ± 0.052	1.069 ± 0.185	10.000 ± 19.217	0.942 ± 0.194
	R^2	0.9798	0.9195	0.9665	0.9338	0.9224	0.7255
	χ^2_{red}	0.0003	0.0511	0.0009	0.0036	0.0144	0.0044
Jain and Snoeyink (J–S) modified extended Langmuir	R^2_i	0.5392	0.7988	0.9048	0.7581	0.7493	0.5281
	$\chi^2_{red,i}$	0.0919	0.0900	0.0282	0.1008	0.1639	0.1418
	R^2_j	0.4798	0.7125	0.9577	0.9793	0.8562	0.8856
	$\chi^2_{red,j}$	0.3541	0.0986	0.0216	0.0123	0.0459	0.4262
P-factor	P_i	4.200	0.879	3.003	2.638	0.995	4.163
	$K_{L,i}$	31.32 ± 2.64	12.52 ± 2.37	23.17 ± 1.59	19.86 ± 2.20	33.15 ± 5.38	60.20 ± 5.98
	a_{Li} (L/mmol)	27.47 ± 2.80	10.47 ± 2.72	20.32 ± 1.70	12.70 ± 1.83	27.72 ± 5.62	38.52 ± 4.55
	R^2	0.9702	0.9588	0.9732	0.9365	0.9211	0.9548
	χ^2_{red}	0.0004	0.0262	0.0007	0.0035	0.0147	0.0007

to obtain Langmuir constants Q_{max} and b, which are shown in Table 5.

Bicomponent adsorption occurred at pH 5.5, 25 °C, and 0.2 g/L STA. Fig. 6d–f shows the plots for binary equimolar adsorption systems Co^{2+}–Cu^{2+}, Co^{2+}–Ni^{2+}, and Cu^{2+}–Ni^{2+}, respectively. Table 5 shows the results of modeling the bicomponent experimental adsorption data with four multicomponent isotherm models (experimental equilibrium data available in Supplementary Table 3). The equilibrium adsorption data for binary metallic systems can also be discussed in terms of maximum adsorption capacity of a metal ion i in the presence of another metal ion j, in comparison, when i is present alone in the aqueous solution ($Q_{max,exp,i,multi}/Q_{max,exp,mono}$). For $Q_{max,exp,i,multi}/Q_{max,exp,mono} > 1$, the adsorption of species i is promoted by the presence of the species j. For $Q_{max,exp,i,multi}/Q_{max,exp,mono} = 1$, there is no noticeable net interaction between i and j. For $Q_{max,exp,i,multi}/Q_{max,exp,mono} < 1$, the adsorption of species i is suppressed by the presence of the species j (Ronda et al., 2013). As can be seen in Table 5, the adsorption of Co^{2+} and Ni^{2+} is suppressed in the presence of Cu^{2+}, whereas the adsorption of Ni^{2+} is favored in the presence of Co^{2+}. The Pearson parameter (δ) for Co^{2+}, Cu^{2+}, and Ni^{2+} is 0.130, 0.104, and 0.126, respectively. These cations are considered as borderline Lewis acids, whereas a carboxylate ligand, such as an acetate ion, is considered as a hard Lewis base. However, the two carboxylate groups from a trimellitate moiety grafted onto STA behave as very weakly basic, negatively charged, oxygen-donor groups that are stabilized by resonance. Thus, based on the experimental multicomponent data, it is possible to conclude that these carboxylate groups have a higher affinity for Cu^{2+} than Ni^{2+} and Co^{2+}. The obtained results are in good agreement with the softness order of metal ions studied ($Cu^{2+} > Ni^{2+} > Co^{2+}$). These results are also in good agreement with the Langmuir constants ($b_{Cu^{2+}} > b_{Co^{2+}} > b_{Ni^{2+}}$), considering the slight difference in the Pearson parameter for Co^{2+} and Ni^{2+} (Table 4). These data also suggest that there is the possibility to separate Ni^{2+} from Co^{2+} and Ni^{2+} from Cu^{2+} using kinetic and thermodynamic control on the basis of kinetic ($k_{2,i}/k_{2,j}$) and isotherm data ($Q_{max,exp,i,multi}/Q_{max,exp,mono}$) using a fixed-bed adsorption column system, controlling the inlet flow rate and concentration of each metal ion. This finding can be very useful for treating effluents from acid mine drainage, industrial wastewaters, and in the pre-concentration steps of hydrometallurgical processes. The adsorption of single, binary, and ternary systems of Co^{2+}, Cu^{2+}, and Ni^{2+} in aqueous solutions using a fixed-bed column is the focus of subsequent parts of this paper.

Factors affecting the preference of STA for a specific metal ion may be related to the characteristics of the adsorption sites, that is, the functional groups present in its surface and the properties of the metal ions in solution (e.g., concentration, ionic size, primary and secondary valence, and coordination number) as well as the solution characteristics (e.g., pH, ionic strength, and presence of different counter ions) (Srivastava et al., 2006).

The values of $\Delta_{ads}G°$ for a multicomponent system were slightly more negative than the $\Delta_{ads}G°$ value of a monocomponent system. The values of $\Delta_{ads}G°$ indicate that adsorption was more favorable in multicomponent systems compared to the monocomponent systems. Considering the values of $\Delta_{ads}G°$, there is no clear experimental evidence for a change in the adsorption mechanism controlling the uptake of metal ions in the binary system in relation to single system. However, in Fig. 6e, it is noticeable that a double layer seems to have been formed, which was indicated by the formation of a second plateau in the isotherm of the Co–Ni binary system. It favored the adsorption of Ni^{2+} rather than Co^{2+}. In binary systems Co–Cu and Cu–Ni, this behavior was not observed.

As can be seen in Table 5, comparing the three binary adsorption systems, higher R^2 and lower χ^2 values were obtained by fitting the modified extended Langmuir and P-factor models to the

experimental adsorption data. Non-modified extended Langmuir and J–S modified extended Langmuir models exhibited a poor fit to the experimental data. These results also confirm that there are interactions between the two metal ions in the three binary adsorption systems. Supplementary Fig. 3 shows the plots of $q_{e,est}$ against $q_{e,exp}$ for the three binary adsorption systems and four competitive adsorption models tested. Supplementary Table 4 shows the slope and the intercept from plots of estimated ($q_{e,est}$) against experimental maximum adsorption capacities ($q_{e,exp}$) for all competitive adsorption models tested. Supplementary Fig. 3a–f shows plots of $q_{e,est}$ versus $q_{e,exp}$ for the three bicomponent systems studied. In these graphs, most of the data points are distributed around the 45° dashed line, with 95% of confidence interval, for modified extended Langmuir and P-factor models. For these models, the slopes and intercepts were closer to unity and zero, respectively, which indicates that these multicomponent models could estimate $q_{e,est}$ from the experimental data very well.

The maximum metal ion adsorption capacities in the binary systems ($Q_{max,exp,i+j}$) (Table 5) were lower than the sum of the single maximum adsorption capacities for each metal ion. Similar results were observed by Srivastava et al. (2006) for the adsorption of Cd^{2+} and Zn^{2+} on bagasse fly ash in mono- and bi-component systems. According to Srivastava et al. (2006), this result may imply that there is a variety of adsorption binding sites on the adsorbent surface exhibiting partially specific affinity to the single metal ions. These conclusions seems to violate the assumptions of the Langmuir isotherm theory, that is, the adsorbent surface is homogeneous, there is no preferential adsorption and lateral interaction between adsorbates, and the affinity of each adsorption site by the adsorbate is uniform. Although the Langmuir isotherm theory fails, to a certain degree, to fully describe the adsorption behavior of binary systems, the use of a modified extended Langmuir model seemed reasonable, as the interaction factor took into account the deviations from the non-modified extended Langmuir model and its assumptions. According to Choy et al. (2000), the P-factor model cannot account for all competitions and interactions that may influence the competitive adsorption, resulting in some deviations between $q_{e,est}$ and $q_{e,exp}$. However, according to analysis by Choy et al. (2000), the P-factor model provides a major enhancement over the data estimated by the extended Langmuir model. The obtained results in this study are in good agreement with the analysis of Choy et al. (2000), as the estimation of q_e values provided by P-factor was better than the extended Langmuir model.

3.3. Desorption and reuse of the spent adsorbent

The desorption of STA-loaded with Co^{2+}, Cu^{2+}, and Ni^{2+} was performed using a batch process at 25 °C and 130 rpm with 20.0 mL of 1.0 mol/L HNO_3 for 5 min. The desorption percentage, E_{des}, was 100% for all metal ions studied. The suggested mechanism for the desorption of metal ions from STA-loaded with Co^{2+}, Cu^{2+}, and Ni^{2+} is that of ion exchange, in which metal ions are exchange by hydronium ions. Desorption tests with 0.05 mol/L $ClCH_2COOH/ClCH_2COONa$ buffer (pH 2) were also performed. These tests revealed that the monochloroacetate/monochloroacetic acid buffer was efficient in desorbing the metal ions from STA. The desorption efficiency attained was about 50%. The reason for the desorption efficiency of the buffer solution being lower than nitric acid solution was the change in the pH of the buffer solution to higher values (pH > 2) during the desorption process. This result proves that ion exchange is the mechanism controlling the desorption process.

FTIR spectra of STA (blank) and STA after desorption of Co^{2+}, Cu^{2+}, and Ni^{2+} were also recorded (Supplementary Fig. 4). The same bands attributed to the success of chemical modification of SB with TA were confirmed in the adsorbents after desorption, which

Table 6
Comparison of Q_{max} for removal of Co^{2+}, Cu^{2+}, and Ni^{2+} by various adsorbents.

Adsorbent	Q_{max} (mmol/g)[a]			Reference
	Co^{2+}	Cu^{2+}	Ni^{2+}	
PET-g-(MAA/AAm)	0.461	0.492	0.741	Coşkun et al. (2006)
Sp–HPBA	0.039	0.043	0.036	Çimen et al. (2013)
Palygorskite (Brazil)	1.604	1.279	0.078	Oliveira et al. (2013)
BANPA	0.56	0.49	0.55	Rodrigues et al. (2013)
BANMA	0.27	0.29	0.47	Rodrigues et al. (2013)
PAMMAm	0.122	0.201	0.104	Kushwaha et al. (2013)
Sil–NSuc	1.85	1.04	1.89	Arakaki et al. (2013)
Celam biopolymer	0.097	0.102	0.077	Silva Filho et al. (2013)
STA	1.140	1.197	1.563	This study

[a] Maximum adsorption capacities obtained from the Langmuir model at 25 °C.

proves that there was no ester bond hydrolysis during desorption experiments. Furthermore, the study of re-adsorption of Co^{2+}, Cu^{2+}, and Ni^{2+} using the spent STA adsorbent demonstrated that the re-adsorption efficiency was 100% for all metal ions studied. These results prove that the STA adsorbent can be recovered and reused without loss in its adsorption capacity. The results of the studies of desorption and re-adsorption demonstrates that it is possible to recover both the metal ions and the STA adsorbent, which improves the economic feasibility of the proposed adsorption process.

3.4. Comparison with previously reported data for Co^{2+}, Cu^{2+}, and Ni^{2+} adsorption

Table 6 shows various adsorbents that have been used to remove Co^{2+}, Cu^{2+}, and Ni^{2+} from aqueous solutions, as reported in previous studies, for comparison purposes. Comparing the STA adsorbent with some previously reported adsorbents used for the removal of Co^{2+}, Cu^{2+}, and Ni^{2+}, it is possible to conclude that the STA adsorbent is one of the most powerful adsorbents synthesized for this purpose.

4. Conclusions

Sugarcane bagasse modified with trimellitic anhydride (STA) was successfully synthesized and characterized by FTIR, elemental analysis, TGA, and PZC measurements. The percent weight gain and number of carboxylic acid groups were found to be 73.9% and 3.78 mmol/g, respectively. The STA adsorbent was efficient in removing Co^{2+}, Cu^{2+}, and Ni^{2+} from single and binary component aqueous solutions. The adsorption kinetics followed the pseudo-second-order model. The experimental data fitted very well to the Langmuir and Sips isotherm models. The equilibrium time obtained from the kinetic study and the monocomponent maximum adsorption capacity determined by Langmuir model for adsorption of Co^{2+}, Cu^{2+}, and Ni^{2+} were 180, 250, and 75 min and 1.140, 1.197, and 1.563 mmol/g, respectively. The bicomponent adsorption studies demonstrated that the adsorption of Co^{2+} and Ni^{2+} is suppressed in the presence of Cu^{2+}, and Ni^{2+} suppresses the adsorption of Co^{2+}. The bicomponent data fitted very well to the modified extended Langmuir and P-factor models. Desorption studies demonstrated that the STA adsorbent can be 100% desorbed and reused.

Acknowledgements

Appendix A. Supplementary data

Supplementary data associated with this article can be found, in the online version, at http://dx.doi.org/10.1016/j.indcrop.2015.05.022

References

Ahmad, P., Prasad, N.V., 2011. Environmental Adaptations and Stress Tolerance of Plants in the Era of Climate Change. Springer, New York.

Amin, N.-U., Hussain, A., Alamzeb, S., Begum, S., 2013. Accumulation of heavy metals in edible parts of vegetables irrigated with waste water and their daily intake to adults and children, district Mardan, Pakistan. Food Chem. 136, 1515–1523.

Arakaki, L.N.H., Filha, V.L.S.A., Germano, A.F.S., Santos, S.S.G., Fonseca, M.G., Sousa, K.S., Espínola, J.G.P., Arakaki, T., 2013. Silica gel modified with ethylenediamine and succinic acid-adsorption and calorimetry of cations in aqueous solution. Thermochim. Acta 556, 34–40.

ATSDR, 2014. Support Document to the 2013 Priority List of Hazardous Substances that will be the Subject of Toxicological Profiles. Division of Toxicology and Environmental Medicine, Atlanta, GA, pp. 1–12 (accessed 21.11.14.) http://www.atsdr.cdc.gov/SPL/resources/ATSDR_2013_SPL_Support_Document.pdf

Barakat, M.A., 2011. New trends in removing heavy metals from industrial wastewater. Arabian J. Chem. 4, 361–377.

Bhatnagar, A., Sillanpää, M., 2010. Utilization of agro-industrial and municipal waste materials as potential adsorbents for water treatment – a review. Chem. Eng. J. 157, 277–296.

Braude, E.A., Nachod, F.C., 1955. Determination of Organic Structures by Physical Methods. Academic Press Inc., New York, USA.

Butler, J.A.V., Ockrent, C., 1930. Studies in electrocapillarity. Part III: the surface tensions of solutions containing two surface-active solutes. J. Phys. Chem. 34, 2841–2859.

Choy, K.K.H., Porter, J.F., McKay, G., 2000. Langmuir isotherm models applied to the multicomponent sorption of acid dyes from effluent onto activated carbon. J. Chem. Eng. Data 45, 575–584.

Çimen, A., Bilgiç, A., Kursunlu, A.N., Gübbük, İ.H., Uçan, H.İ., 2013. Adsorptive removal of Co(II) Ni(II), and Cu(II) ions from aqueous media using chemically modified sporopollenin of Lycopodium clavatum as novel biosorbent. Desalin. Water Treat. 52, 4837–4847.

Coşkun, R., Soykan, C., Saçak, M., 2006. Adsorption of copper(II), nickel(II) and cobalt(II) ions from aqueous solution by methacrylic acid/acrylamide monomer mixture grafted poly(ethylene terephthalate) fiber. Sep. Purif. Technol. 49, 107–114.

Ferreira, B.C.S., Teodoro, F.S., Mageste, A.B., Gil, L.F., de Freitas, R.P., Gurgel, L.V.A., 2015. Application of a new carboxylate-functionalized sugarcane bagasse for adsorptive removal of crystal violet from aqueous solution: kinetic, equilibrium and thermodynamic studies. Ind. Crops Prod. 65C, 521–534.

Foo, K.Y., Hameed, B.H., 2010. Insights into the modeling of adsorption isotherm systems. Chem. Eng. J. 156, 2–10.

Freundlich, H.M.F., 1906. Over the adsorption in solution. Z. Phys. Chem. Stoch Ve 57, 385–470.

Fu, F., Wang, Q., 2011. Removal of heavy metal ions from wastewaters: a review. J. Environ. Manage. 92, 407–418.

Harris, D.C., 2010. Quantitative Chemical Analysis, 8th ed. W.H. Freeman, New York.

Haynes, W.M., 2014. CRC Handbook of Chemistry and Physics, 95th ed. Taylor & Francis.

Ho, Y.S., McKay, G., 1998. Kinetic models for the sorption of dye from aqueous solution by wood. Process Saf. Environ. Prot. 76, 183–191.

Ho, Y.S., McKay, G., 1999. Pseudo-second order model for sorption processes. Process Biochem. 34, 451–465.

Húmpola, P.D., Odetti, H.S., Fertitta, A.E., Vicente, J.L., 2013. Thermodynamic analysis of adsorption models of phenol in liquid phase on different activated carbons. J. Chil. Chem. Soc. 58, 1541–1544.

Jain, J.S., Snoeyink, V.L., 1973. Adsorption from bisolute systems on active carbon. J. Water Pollut. Control Fed. 45, 2463–2479.

Karnitz, O., Gurgel, L.V.A., de Freitas, R.P., Gil, L.F., 2009. Adsorption of Cu(II) Cd(II), and Pb(II) from aqueous single metal solutions by mercerized cellulose and mercerized sugarcane bagasse chemically modified with EDTA dianhydride (EDTAD). Carbohydr. Polym. 77, 643–650.

Kazemipour, M., Ansari, M., Tajrobehkar, S., Majdzadeh, M., Kermani, H.R., 2008. Removal of lead, cadmium, zinc, and copper from industrial wastewater by carbon developed from walnut, hazelnut, almond, pistachio shell, and apricot stone. J. Hazard. Mater. 150, 322–327.

Klaassen, C., 2008. Casarett & Doull's Toxicology: The Basic Science of Poisons: The Basic Science of Poisons, 7th ed. McGraw-Hill, New York.

Kumar, U., 2006. Agricultural products and by-products as a low cost adsorbent for heavy metal removal from water and wastewater: a review. Sci. Res. Essays 1, 33–37.

Kushwaha, A.K., Gupta, N., Chattopadhyaya, M.C., 2013. Dynamics of adsorption of Ni(II) Co(II) and Cu(II) from aqueous solution onto newly synthesized poly[N-(4-[4-(aminophenyl) methylphenylmethacrylamide])]. Arabian J. Chem. http://dx.doi.org/10.1016/j.arabjc.2013.1006.1007

Lagergren, S.Y., 1898. Zur Theorie der sogenannten Adsorption gelöster Stoffe, Kungliga Svenska Vetenskapsakademiens, 24. Handlingar, pp. 1–39.

Langmuir, I., 1918. The adsorption of gases on plane surfaces of glass, mica and platinum. J. Am. Chem. Soc. 40, 1361–1403.

Liu, Y., 2009. Is the free energy change of adsorption correctly calculated? J. Chem. Eng. Data 54, 1981–1985.

Łyszczek, R., 2007. Thermal and spectroscopic investigations of new lanthanide complexes with 1,2,4-benzenetricarboxylic acid. J. Therm. Anal. Calorim. 90, 533–539.

Mathews, A.P., Weber, W.J., 1980. Mathematical modeling of adsorption in multicomponent systems, adsorption and ion exchange with synthetic zeolites. Am. Chem. Soc. 135, 27–53.

McKay, G., Al Duri, B., 1987. Simplified model for the equilibrium adsorption of dyes from mixtures using activated carbon. Chem. Eng. Process. Process Intensif. 22, 145–156.

Miretzky, P., Cirelli, A.F., 2010. Cr(VI) and Cr(III) removal from aqueous solution by raw and modified lignocellulosic materials: a review. J. Hazard. Mater. 180, 1–19.

Nada, A.-A.M.A., Hassan, M.L., 2006. Ion exchange properties of carboxylated bagasse. J. Appl. Polym. Sci. 102, 1399–1404.

Noh, J.S., Schwarz, J.A., 1990. Effect of HNO_3 treatment on the surface-acidity of activated carbons. Carbon 28, 675–682.

Oliveira, A.B.M., Coelho, L.O., Gomes, S.S., Costa, I., Fonseca, M., de Sousa, K., Espínola, J.P., da Silva Filho, E., 2013. Brazilian palygorskite as adsorbent for metal ions from aqueous solution – kinetic and equilibrium studies. Water Air Soil Pollut. 224, 1–13.

Pavia, D., Lampman, G., Kriz, G., Vyvyan, J., 2009. Introduction to Spectroscopy, 4th ed. Cengage Learning, Belmont, USA.

Pośpiech, B., Walkowiak, W., 2007. Separation of copper(II), cobalt(II) and nickel(II) from chloride solutions by polymer inclusion membranes. Sep. Purif. Technol. 57, 461–465.

Redlich, O., Peterson, D.L., 1959. A useful adsorption isotherm. J. Phys. Chem. 63, 1024.

Rocha, G.J.D.M., Nascimento, V.M., Gonçalves, A.R., Silva, V.F.N., Martín, C., 2015. Influence of mixed sugarcane bagasse samples evaluated by elemental and physical–chemical composition. Ind. Crops Prod. 64, 52–58.

Rodrigues, N.F.M., Santana, S.A.A., Bezerra, C.W.B., Silva, H.A.S., Melo, J.C.P., Vieira, A.P., Airoldi, C., Silva Filho, E.C., 2013. New chemical organic anhydride immobilization process used on banana pseudostems: a biopolymer for cation removal. Ind. Eng. Chem. Res. 52, 11007–11015.

Ronda, A., Martín-Lara, M.A., Dionisio, E., Blázquez, G., Calero, M., 2013. Effect of lead in biosorption of copper by almond shell. J. Taiwan Inst. Chem. Eng. 44, 466–473.

Saikia, C.N., Dutta, N.N., Borah, M., 1993. Thermal behaviour of some homogeneously esterified products of high α-cellulose pulps of fast growing plant species. Thermochim. Acta 219, 191–203.

Silva Filho, E.C., Santos Júnior, L.S., Silva, M.M.F., Fonseca, M.G., Santana, S.A.A., Airoldi, C., 2013. Surface cellulose modification with 2-aminomethylpyridine for copper cobalt, nickel and zinc removal from aqueous solution. Mater. Res. 16, 79–84.

Sips, R., 1948. On the structure of a catalyst surface. J. Chem. Phys. 16, 490–495.

Soetan, K., Olaiya, C., Oyewole, O., 2010. The importance of mineral elements for humans, domestic animals and plants: a review. Afr. J. Food Sci. 4, 200–222.

Srivastava, V.C., Mall, I.D., Mishra, I.M., 2006. Modelling individual and competitive adsorption of cadmium(II) and zinc(II) metal ions from aqueous solution onto bagasse fly ash. Sep. Sci. Technol. 41, 2685–2710.

Srivastava, V.C., Mall, I.D., Mishra, I.M., 2009. Competitive adsorption of cadmium(II) and nickel(II) metal ions from aqueous solution onto rice husk ash. Chem. Eng. Process. Process Intensif. 48, 370–379.

Sun, R.C., 2010. Cereal Straw as a Resource for Sustainable Biomaterials and Biofuels: Chemistry, Extractives, Lignins, Hemicelluloses and Cellulose, 1st ed. Elsevier, Oxford, UK.

Varhegyi, G., Antal, M.J., Szekely, T., Szabo, P., 1989. Kinetics of the thermal decomposition of cellulose, hemicellulose, and sugarcane bagasse. Energ Fuel 3, 329–335.

Vieira, R.S., Beppu, M.M., 2006. Interaction of natural and crosslinked chitosan membranes with Hg(II) ions. Colloids Surf. A 279, 196–207.

Wan Ngah, W.S., Hanafiah, M.A.K.M., 2008. Removal of heavy metal ions from wastewater by chemically modified plant wastes as adsorbents: a review. Bioresour. Technol. 99, 3935–3948.

Yavuz, Ö., Altunkaynak, Y., Güzel, F., 2003. Removal of copper, nickel, cobalt and manganese from aqueous solution by kaolinite. Water Res. 37, 948–952.